A Thermodynamically Consistent Force Field for Molecular Dynamics Simulations of Alkaline-Earth Carbonates and Their Aqueous Speciation

Paolo Raiteri, Raffaella Demichelis and Julian D. Gale*

Nanochemistry Research Institute, Curtin Institute for Computation, and Department of Chemistry, Curtin University, GPO Box U1987, Perth, WA 6845, Australia

KEYWORDS

Alkaline-earth carbonates, ion-pairing, force field, molecular dynamics, free energy

ABSTRACT

In recent years atomistic simulations have become increasingly important in providing molecular insight to complement experiments. Even for the seemingly simple case of ion-pair formation a detailed atomistic picture of the structure and relative stability of the contact, solvent-shared and solvent-separated ion-pairs can only be readily achieved by computer simulation. Here a new force field parameterization for the alkaline-earth carbonate interactions in water has been developed by fitting against experimental thermodynamic and structural data. We

demonstrate that the present force field can accurately reproduce the dynamics and thermodynamics of the ions in solution, which is the key to producing quantitatively accurate data that can be compared against experiment.

INTRODUCTION

Alkaline-earth metals play an important role in many biological, mineralogical and industrial processes, and in water they are usually found as di-cations. In aqueous environments they can also bind with multiply charged anions, such as phosphate, sulfate and carbonate, ultimately leading to precipitation from solution as crystalline or amorphous phases under appropriate supersaturation.

In the past decade, since the existence of stable pre-nucleation clusters was first suggested for $CaCO_3$ and possibly other minerals,[1,2] the early stages of ion association have come under considerable scrutiny both experimentally and computationally. The size and lifetime of these clusters are such that they remain difficult to probe with many experimental techniques. Direct structural characterization with atomic resolution therefore appears not to be currently feasible, and so simulation has played an important role in filling this void and in providing quantitative support for the available experimental information.

Studying the properties of pre-nucleation clusters is also challenging from a modeling perspective. In the case of *ab initio* methods, where systems of only a few nanometers in size can be simulated for just tens to hundreds of picoseconds, a direct simulation of ion aggregation, nucleation and growth is far beyond what can be achieved in the near future. On the other hand, force field simulations are computationally much less expensive and can already generate μs-long atomistic trajectories for systems with sizes and concentrations comparable with experiment.[3]

That said, there is a risk that force field simulations can lack sufficient accuracy and may provide unreliable predictions of the thermodynamics and kinetics of systems. However, it is our contention that if a force field is carefully calibrated against experimental thermodynamic data, it can be an extremely powerful tool to study the very early stages of aggregation and, with the aid of advanced sampling techniques, of the nucleation process itself.

The key first step toward accurate force field simulations of any system lies in the choice of the functional form and parameterization. There are already numerous parameter sets in the literature for alkaline-earth cations in water,[4-10] and similarly many force fields also exist for their carbonate salts in the solid-state.[11-17] However, the number of models that are capable of consistently describing both the ions in the solid-state and in aqueous solution is more limited.[18-22] One such parameterization involves the inclusion of polarisability for oxygen via the shell model for water and carbonate of de Leeuw and Parker.[18,23] Unfortunately this water model has been shown to freeze at room temperature,[24] with the melting point having been computed to be close to 390 K.[25] This potential was subsequently modified by Kerisit and Parker[26] to resolve this issue. However, the water structure is still at odds with experiment with a reported equilibrium density of 1.27 g/cm^3 and a distorted hydrogen bond network which result in a first peak of the pair distribution function that is too broad and integrates to ~12 molecules (see Fig S1 in the supplementary information). Given this discrepancy, it appears likely that any results obtained with such model would be substantially in error with regard to the hydration structure.

For the case of the aqueous $CaCO_3$ system, it has been recently shown that it is essential to ensure that the thermodynamics of the model are taken into account

during parameterization;[20] something that has been widely overlooked in both previous and even subsequent works. Based on such models it is then possible to obtain results for solution speciation that are in good quantitative agreement with experimental data.[3]

In the present study we build on our earlier model for $CaCO_3$ as a starting point[3] and extend it to include Mg^{2+}, Sr^{2+} and Ba^{2+} using the same thermodynamically-motivated approach. We should note that Tomono *et al*.[22] have also recently published an extension of one of our models to this system, based on the use of a rigid water molecule. However, they determined the parameters for Mg^{2+} through the use of scaling arguments with reference to an earlier potential model, rather than by following the methodology that was used for Ca^{2+}. As a result the model has been primarily tested for structural properties. The only validation of the thermodynamics against experiment was for the enthalpy of cation exchange between the solid and aqueous solution. For ions in aqueous solution we argue that it is important to calibrate against free energies, rather than enthalpies, since the entropic contribution cannot be ignored. For this reason we have derived a new force field that aims to reproduce the experiment solubility of alkaline-earth carbonates and is therefore grounded in the free energies of the relevant systems. As a starting point for the development of the new force field we use the parameters from our previous work on calcium carbonate[3]. Therefore the carbonate intramolecular parameters, including the partial charges, as well as the calcium-water and calcium-carbonate intermolecular interactions, are all left unchanged. Below we describe the parameterization process in detail and then discuss the application of the new force field to the free energy landscape for ion-pairing.

COMPUTATIONAL METHODOLOGY

In the first step of the parameterization the cation-water interactions were fitted against the experimental estimates of their hydration free energies as reported by David *et al*..[27] In order to adjust the cation-water parameters we performed long molecular dynamics simulations (MD) in a 49.843 Å box of SPC/Fw[28] water (4,177 molecules) with the LAMMPS code[29]. The hydration free energy was calculated using the free energy perturbation (FEP) technique[30,31] by progressively switching off the electrostatic and the van der Waals interactions between the ions and water. Each interaction was turned off in 20 stages and the free energy contribution of each stage was obtained from a 2 ns production run, after 200 ps of equilibration, which equates to a total of 80 ns for each production phase. The calculated hydration free energy was then corrected for finite size effects by applying all the relevant contributions, as per our previous work.[20,32] Further technical details of the molecular dynamics simulations are given later.

In the second step, the interaction between the cations and carbonate were determined by using a relaxed fit[33] to the structures, as well as the experimental bulk moduli, within the program GULP.[34] The structures of magnesite ($MgCO_3$) and dolomite ($MgCa(CO_3)_2$) were taken from Markgraf and Reeder,[35,36] strontianite ($SrCO_3$) from Antao and Hassan,[37] and witherite ($BaCO_3$) at 0 GPa from the variable pressure study due to Holl *et al*.[38] Here it should be noted that magnesite and dolomite adopt essentially the same underlying rhombohedral structure as calcite, while the two alkaline-earth carbonates containing the larger metal cations adopt an orthorhombic crystal structure, analogous to the aragonite polymorph of calcium carbonate. The bulk moduli for the heavier alkaline-earth carbonates were taken to be 58(10) GPa

and 50(8) GPa for strontianite and witherite, respectively, though we note there is some variability in the experimental results.[39] For magnesite, dolomite and calcite the bulk moduli quoted are due to Fiquet *et al*,[40] Ross and Reeder,[41] and Zhang and Reeder,[42] respectively.

Having fitted the thermodynamics of the ions in solution correctly, the free energies of the crystalline carbonate phases at 298.15 K were also included in the observables to ensure that the solubility products of these minerals would be as close as possible to the experimental values. Here the lattice free energies were computed within the quasi-harmonic approximation with a shrinking factor of 8 in all directions to sample the phonons within the Brillouin zone using a Monkhorst-Pack mesh. For consistency with classical molecular dynamics simulations of the ions in solution, the zero point energy was excluded from the free energy of the solid phases during the lattice dynamics calculations. Corrections for the free energies of the isolated ions in the gas phase were added to the lattice free energy to complete the Born-Haber cycle.

The final set of parameters developed in this work is given in Table 1, together with the equivalent values for Ca^{2+} previously reported. It should be noted that there is a small change in the carbonate-water interaction parameters reported here relative to our earlier works. This was made to improve the description of the hydration of the carbonate anion and its free energy of solvation.

All the MD simulations, including the FEP calculations, used a 1 fs time step, which led to good energy conservation in control NVE runs, a 100 fs relaxation time for the length 5 Nosé-Hoover chain thermostat,[43,44] and the reciprocal space electrostatics were calculated using the PPPM algorithm with an accuracy of 10^{-5}. LAMMPS was then augmented by applying the PLUMED 2.0 plug-in[45] in order to

calculate the cation-carbonate pairing free energies with the metadynamics technique.[46] As collective variables (CVs) we used the cation-carbon distance and the cation-water coordination number (CN), which was defined using the continuous differentiable function;

$$CN = \sum_i \frac{1 - \left(\frac{r_i - d_0}{r_0}\right)^n}{1 - \left(\frac{r_i - d_0}{r_0}\right)^m} \quad (1)$$

where r_0=1.0 Å for all ions (except Mg^{2+} where r_0=1.2 Å), n=4, m=8 and r_i is the distance between the cation and the oxygen of *i-th* water molecule. We also used different values of d_0 for each cation, to reflect the varying positions of the first peak of the pair distribution function with the water oxygen (1.9 Å for Mg^{2+}, 2.1 Å for Ca^{2+}, 2.3 Å for Sr^{2+} and 2.5 Å for Ba^{2+}).

The ion-pairing free energy profiles were constructed by running metadynamics simulations with Gaussians laid every 1 ps and with an initial height equal to k_BT. The Gaussian widths were 0.2 Å and 0.1 along the distance and coordination number CVs, respectively. In order to ensure convergence of the final free energy we ran 30 parallel simulations using the multiple-walkers algorithm[47] for a total simulation time of approximately 250 ns and we employed the well-tempered technique[48] with a bias-factor of 5 to progressively reduce the heights of the Gaussians until convergence.

RESULTS AND DISCUSSION

BULK PHASES. The optimized lattice parameters, bulk moduli and free energies of dissolution for the mineral phases used in the current parameterization are given in Table 2. We note upfront that much of this information was used during the fitting

procedure and therefore the level of agreement should not be totally unexpected. That said, for each alkaline-earth cation included there were only two free parameters within the fitting process for the solid phases, namely the A and ρ of Buckingham potential between the metal and oxygen of carbonate, and so some degree of compromise is necessary. In the present work the emphasis is placed upon obtaining the correct relative thermodynamics of species in the crystalline state and solution, followed by the structure, with the mechanical properties carrying the lowest weight. Hence, the consistent overestimation of the bulk moduli relative to experiment is to be expected, and is typical of many fully charged ionic models. In contrast, the lattice parameters are generally well reproduced with most deviations being less than 0.5%. The largest error is for witherite, where the b parameter is under estimated by 1.3%, while c is overestimated by almost the same amount leading to a, fortuitously, accurate volume for the mineral.

In Table 2 we also report the linear thermal expansion coefficients for the minerals, which overall agree well with the experiments. In particular, we note that this force field reproduces the negative linear expansion coefficient of the calcite a axis at low temperature and that all the hexagonal crystals display greater expansion in the c direction than in a. For the orthorhombic phases, there is a similar trend with the thermal expansion parallel to the c axis being well reproduced, since this also corresponds to the direction normal to the plane of the carbonate anions as per the hexagonal c axis. This suggests that the force field reported here is also reliable for properties that go beyond the initial parameterization.

Results for the thermodynamics of mineral dissolution are given in Table 2. These values were used as part of the training data for the derivation of the force field

and so, as expected, most of the calculated dissolution free energies are within 2 kJ/mol of the experimental values. It should be noted that there is a statistical uncertainty in these values arising from the free energy of hydration of the cations and carbonate in solution. Despite performing new longer free energy perturbation simulations relative to our previous works, the residual uncertainty is of the order of the ambient thermal energy. Hence a discrepancy of 2 kJ/mol is within this statistical uncertainty. There is one case where the deviation exceeds this and therefore requires further comment. For the case of calcite the discrepancy is just in excess of 3 kJ/mol, which is increased relative to our previous estimate due to a shift of 1 kJ/mol in the solvation free energy of Ca^{2+} as a result of the longer simulations. However, we prefer not to change the parameterization for the interactions in calcium carbonate polymorphs since the model is also constrained by the need to accurately reproduce the relative stability of calcite versus aragonite. It should also be noted that the free energy of dissolution for dolomite was not fitted, but is still in good agreement with experiment. That said, there is considerable variability in the solubility of dolomite due to variation in the stoichiometry away from the ideal composition, as well as due to cation disorder.[49] Here we have chosen an experimental solubility for ordered dolomite, which resembles the model adopted for the present calculations.

SOLUTION PROPERTIES OF INDIVIDUAL IONS. The hydration, structural and dynamic properties of the cations in aqueous solution computed using the final set of force field parameters are given in Table 3. The free energies of hydration were included in the training set used for force field fitting and therefore it is no surprise that they agree well with the experimental values. However, the majority of the quantities given in Table 3 were not part of the training set and therefore provide a strong validation of the present parameterization. When compared to previous force-

fields for the alkaline earth metal cations that are available in the literature[10,50,51] the present parameterization performs comparably to, or better than these prior models in reproducing the position of the water solvation shell, the coordination number, the ion self-diffusion coefficient and the water residence time. It is also worth noting here that for Ca^{2+} and Mg^{2+} the water structure around the ion is consistent with that predicted by the variable charge force-field of Yang and Li[52], where polarization effects are effectively taken into account. Yang and Li[52] also predict the solvation free energies for Ca^{2+} and Mg^{2+} to be slightly less negative (-1424 kJ/mol and -1722 kJ/mol, respectively) than the literature values, including those used to fit our force-field, but it is unclear which perturbation method they used to calculate these free energies and if any correction terms were accounted for. Similarly, the present parameterization performs comparably to previous force-fields for carbonate that are available in the literature[19,53] and have been tested in ref 20, though we note that there is a paucity of good experimental data for this anion.

For all cations, the position of the first peak of the oxygen pair distribution function ($r_{Ca/Mg\text{-}Ow}$) predicted by the present parameterization is slightly closer than the experimental values (by up to ~0.15 Å). This is probably due to the lack of the inclusion of electronic polarizability in the SPC/Fw water model that we employed. Despite the flexibility of the water potential, the moderate distortion of the water molecules in the first hydration shell of the cation cannot increase the water dipole moment sufficiently to compensate for the lack of polarization, and so a shorter cation-water distance is required to reproduce the experimental hydration free energies. The water structure obtained by the present force-field for aqueous Ba^{2+} is also consistent with recent *ab-initio* molecular dynamics simulations[54] that predict the cation-water peak position to be at 2.8Å and a coordination number of 8. It is worth

noting here that there is a large variability in the experimental numbers, which may due to differences in the conditions used, as well as the complexity of the measurements. Although, some of the techniques may be more accurate than others in obtaining the coordination number and cation-oxygen distance it is beyond the scope of this work to assess the experimental literature.

In the case of Mg^{2+} we did not observe any water exchange events in unbiased simulations through out the duration of 50 ns and advanced computational techniques, such as Forward Flux[55,56] or metadynamics,[57] would be required to reliably calculate the water exchange rate around the Mg^{2+} cation, which is beyond the scope of this work. However, our estimates of the barrier height for water exchange at Mg^{2+} (+53 ± 3 kJ/mol, see Figure S1 in the supplementary information) are in line with those from previous force fields (40-55 kJ/mol),[58] though slightly higher than the experimental value (40 kJ/mol) determined from ^{17}O NMR.[59]

The self-diffusion coefficient of the cations has been calculated with three different box sizes (~25 Å, ~50 Å and ~100 Å) and then extrapolated to infinite size to remove finite size effects as shown to be important by Yeh and Hummer[60] (Fig. 1). All the calculated values are slightly larger than the experimental values, but we argue that this is a reflection of the self-diffusion coefficient of SPC/Fw water (D_0=2.86x10^{-5} cm^2/s), which is approximately 25% larger than the experimental value after correction for finite size effects (Fig. 1).

In order to further probe the strength of the water-Mg^{2+} coordination, we performed an extra 50 ns MD run starting from a pre-formed ion-pair, $MgCO_3^{(0)}{}_{(aq)}$. During this simulation Mg^{2+} displayed only its preferred 6-fold coordination with respect to oxygen, where 5 oxygen atoms belonged to water molecules and one to

carbonate. During the whole 50 ns of the simulation no water exchange was observed, while the carbonate displayed relatively fast rotation around the carbon atom and all three oxygen atoms contributed equally to the completion of the Mg^{2+} coordination shell. It is, however, possible that the water exchange rate around magnesium is faster when bound to carbonate, although still outside of the timescales normally accessible by MD.

The cation-water coordination number is also in good agreement with experimental estimates, though these generally have a large uncertainty. From the metadynamics simulations used to compute the ion-pair free energy, discussed below, we could also extract thermodynamic information on the accessible coordination states for the cations (Fig. 2), which will prove useful for the discussion of the ion-pairing process. In the case of Mg^{2+} only 6-fold coordination with water is accessible, with all the other configurations too high in free energy to be visited. However, the situation is different for the other 3 cations, where multiple coordination geometries are accessible at room temperature. In the case of Ca^{2+} the most likely coordination number is 7, however the 8-fold coordination state is only ~4 kJ/mol less stable and separated by a ~12 kJ/mol barrier. The 6-fold coordination state is also a free energy minimum, but it is substantially higher in free energy (12 kJ/mol) and separated by a barrier of about 20 kJ/mol, which lowers the contribution to the average hydration state. For Sr^{2+} the most likely coordination number is 8, with 7 and 9 both about 11 kJ/mol higher in free energy and all thermally accessible. Finally, for Ba^{2+} it is equally probable to have a coordination number of 8 or 9, with the two states separated by a barrier of about 8 kJ/mol. This gives rise to average coordination numbers of 6.0, 7.2, 8.0 and 8.6 for Mg^{2+}, Ca^{2+}, Sr^{2+} and Ba^{2+}, respectively, which are in good agreement with the experimental estimates (Table 3). The position of the first peak of the

carbonate water coordination number is also in good agreement with neutron diffraction experiments by Kameda *et al*.,[61] although it is worth nothing that the measurements had been performed at very high concentration (~3M) while our simulations are effectively at infinite dilution. At such high concentration there are approximately 9 water molecules per carbonate ion and that is probably the reason behind the discrepancy between the measured (9.1) and calculated (12.1) average coordination number of carbonate.

As a final assessment of the parameterization of the force field for the isolated metal cations in water, we have computed the temperature-dependence of the free energy of hydration in the range of 290 – 350 K. All cations yield a good fit to a linear dependence of the free energy on temperature (see Figure S2 in the supplementary information) and thus it is possible to separate the contributions due to the enthalpy and entropy of hydration. These values are also given in Table 3. It should be noted here that the values of the free energy used to derive the parameterization of the force field for the alkaline earths were taken from the work of David *et al* for consistency with our previous derivation for Ca^{2+}. However, since temperature-dependent data was not included in this study, this was taken from an alternative source where there was a systematic shift in the free energy relative to the fitted values, leading to what seems like an inconsistency in Table 3. This offset is predominantly due to differences in the enthalpy of hydration. In contrast, the entropies of hydration show good agreement with the estimates due to Marcus,[62] despite not being fitted, with the largest discrepancy being 24 J/K/mol (~9%) for Ca^{2+}. The hydration enthalpy and entropy of carbonate were also calculated using the same procedure. Here we obtained ΔG_{hyd}=-1312 kJ/mol, ΔH_{hyd}=-1390 kJ/mol and ΔS_{hyd}=-260 J/mol K, which are in excellent agreement with the estimates reported by

Marcus[62] (ΔG_{hyd}=-1315 kJ/mol, ΔH_{hyd}=-1395 kJ/mol and ΔS_{hyd}=-264 J/mol K). In this case the hydration free energy used in the parameterization is also from this source, hence there is no offset to be considered for the enthalpy term.

ION-PAIRING. Having validated the underlying force field model for the isolated ions, we now turn to consider the process of ion-pairing. In Fig. 3 we report the 2D free energy maps for the formation of an ion-pair with the carbonate ion calculated using multiple-walker[47] well-tempered metadynamics[48] as a function of the cation–carbon distance and of the cation–water coordination number. All free energy plots in Fig. 3 show a monotonous profile upon reduction of the cation-carbonate distance until the solvation shells of the two ions come into contact and, at a distance of ~7 Å, a solvent separated ion-pair (SSIP) is formed. Upon further reduction of the cation-carbon distance to ~5 Å the two hydration shells fuse together to form a solvent shared ion-pair (SSHIP), where the ions are separated by only one layer of water molecules. If one of the shared water molecules is displaced by the carbonate then initially a mono-dentate contact ion-pair (CIP) is formed; should a second shared water molecule be displaced then a bi-dentate ion-pair is formed, with a correspondingly shorter metal-carbon distance. This mechanism for the ion-pair formation ensures that the cation always has one of its preferred coordination numbers with respect to the oxygen atoms, which can either belong to the water or to the carbonate (Figure 4). Notably for all the cations the coordination number by water remains largely unchanged until the SSHIP is formed, which is consistent with the carbonate having a more labile hydration shell and being the first one to lose a water molecule in forming the SSHIP.

In the case of Mg^{2+}, only a 6-fold coordination with oxygen is thermodynamically accessible and to form the CIP a molecule from the Mg^{2+} hydration shell has to be displaced, which is an activated process with a free energy barrier between the SSHIP and the CIP of ~25 kJ/mol. This is clearly shown in Figures 3 and 5, where the minimum free energy paths (red and black circles, respectively) are superimposed on the 2D free energy profiles. For Ca^{2+}, Sr^{2+} and Ba^{2+}, these cations can accommodate an extra oxygen in their hydration shell for a relatively small energetic cost and therefore a CIP can be formed without crossing a high free energy barrier. However, the lowest free energy state for the CIP corresponds to a configuration where the cation has lost one water molecule from its hydration shell and recovered its preferred coordination number with respect to oxygen. These are also activated processes for Ca^{2+}, Sr^{2+} and Ba^{2+}, but the height of the barrier decreases as the cations get larger and their hydration free energies less exothermic. The size of Ba^{2+} is such that it can equally accommodate 7 or 8 water molecules even when the CIP is formed, with both states being equally probable.

The ion-pairing of Mg^{2+}, Ca^{2+} and Sr^{2+} with both bicarbonate and carbonate has been previously studied using first principles based on the generalized gradient approximation.[63] While both first principles and the present force field agree that carbonate is preferentially monodentate when ion-pairing with the alkaline earths, several differences are also evident, especially for the hydration state of the cations in the CIP. In particular, the average coordination number of Mg^{2+} was found to be 5.4, implying that the binding of carbonate leads to the displacement of 2 water molecules from the cation, whereas only 1 is lost in the present work. There are several possible reasons for this difference, other than a limitation of the force field parameterization. In particular, there was no specific enhanced sampling of the cation-water

coordination number in the first principles study and so it is unlikely that statistic convergence was obtained during the ~20 ps for which it was feasible to run at the time. In addition, the first principles simulations were run at 400 K, rather than ambient conditions, to try to overcome the systematic over-structuring of water known to occur for water at the level of theory used. However, increasing the temperature also increases the entropic driving force for loss of water and so the discrepancy may simply reflect the different conditions considered. A further point of disagreement between these first principles results and the present work is in regard to the stability of the $SrCO_3$ ion-pair, which in the former case spontaneously dissociates after ~12 ps, while the force field suggests that it should be a distinct local minimum. Again the influence of limited statistics and temperature differences may be important.

Although the main focus here is on the ion-paired states, it is also important to ensure that the free energy profiles are valid in the long-range limit, such that they show the correct asymptotic behavior. If we consider two doubly charged point particles interacting via a screened electrostatic potential (ε_r=79.6 to be consistent with the SPC/Fw water model at 298.15 K) and a repulsive short range potential, we can analytically calculate the system free energy as a function of the distance between the particles and use this to confirm that the well-tempered metadynamics results for both the all atom and simplified two particle simulations correctly reproduce the analytic solution of the problem for the dissociation limit (see Figure S3 in the supplementary information). We note that, within statistical noise, the three curves perfectly overlay beyond ~10 Å and that, after the electrostatic interaction has become negligible compared to the thermal energy, the free energy curve decays monotonically as $-k_B T \ln(4\pi r^2)$. This term is the configurational entropy of the

system and implies that the absolute free energy difference between a bound and unbound ion-pair depends only on the volume available to the species.

It is worth commenting here on the importance of using the cation coordination number as a second collective variable. In fact, if only the cation-carbon distance were to be used in the metadynamics calculations (or with any other free energy technique that relies upon the correct identification of the reaction coordinate to be used as a CV) one would obtain a free energy profile given by the dashed lines in Fig. 5. By comparing the minimum free energy path (dots in Figures 3 and 5) and the 1D pairing free energy profile (dashed line in Figure 5) it is evident that some free energy barriers are not present in the 1D profile. This is particularly critical for the case of Mg^{2+}, where the transition from SSHIP to CIP appears almost barrier-less in the 1D profile, while in reality there is a significant 25 kJ/mol barrier related to removing one water molecule from the Mg^{2+} hydration shell. This is due to the fact that two free energy basins (SSHIP and CIP) overlap along a hidden reaction coordinate (coordination number) and only the minimum free energy value from either of the two basins appears in the 1D profile along the Mg^{2+}-carbon distance. This is a general problem intrinsic to all techniques that require the choice of CVs to calculate free energy profiles (metadynamics, Umbrella Sampling, Steered MD etc.) when an important (*slow*) degree of freedom is missed, while other approaches such as the String Method[64,65] and Transition Path Sampling[66] may not suffer from this issue. The same artifact is present in the case of the other cations, but here the hidden free energy barrier is small (< 8 kJ/mol) and can be readily overcome by thermal fluctuations. Therefore, in these cases the coordination number can be safely neglected in any studies involving the formation and dissociation of any ion-pairs, as shown for example in ref 3.

Now that we have described the importance of choosing the correct number and type of CVs for our free energy calculations, as well as having validated the long-range limiting behavior, we can turn our attention to how our theoretical predictions compare with the experimental estimates. First of all it is worth noting that the very low solubility of the alkaline-earth carbonates prevents the use of many experimental techniques, such as dielectric relaxation spectroscopy,[67] to determine the ion-pairing equilibrium constants and thereby the free energy, which instead has to be inferred by measuring the residual free ion concentrations in solution either by titration methods or ion selective electrode measurements.[68] These experimental techniques rely on the choice of a model that accounts for the possible equilibria in solution, which, particularly in the case of $CaCO_3$, may be more complex than for other species.[1,3] Moreover, for ion-selective electrode measurements it is not clear whether species like the SSHIP or the SSIP are recorded as bound or separated. The standard pairing free energy can be calculated from the measured dissociation constant using the relationship:

$$K_{dis} = \exp(-\Delta G_{dis}/k_B T). \quad (2)$$

From a computational perspective, the first and most straightforward approach one can devise to calculate the dissociation free energy is to directly measure the height difference between states from the free energy landscape. However, there is some ambiguity in the choice of the distances at which the ion-pair can be considered completely dissociated. To be consistent with the experimentally reported pairing free energies, one could think of measuring the free energy difference between the bound state and a state corresponding to the average distance of the ions at 1 M standard concentration. However, apart from for the ideal gas case, this is an ill-defined

distance and in many solid-state physics books one can find two popular approximations for this quantity depending on the assumed packing of the particles; namely the cubic root of the inverse particle number density and the Wigner-Seitz radius, which differ by a factor of ~1.6. In fact, the former corresponds to the radius of a sphere of the volume available to the ions, while the latter is the side of the cube with the same volume. For the case of a 1 M solution these two assumptions yield approximate values of 7.3 Å and 11.8 Å, respectively. The free energy profiles in the region between these two distances (see Figure 3) are still structured due to the presence of explicit water molecules surrounding the ions and this could lead to a large uncertainty in the measured value. A somewhat less ambiguous definition would be to choose the maximum point of the free energy barrier between the bound and dissociated states that we can obtain from the analytic calculations. However, this has no explicit connection to the system concentration. The maximum in the free energy curve is located at a distance, R_{max}=14 Å, where the attractive electrostatic force is exactly counterbalanced by the entropic force that tends to separate the ions;

$$\frac{\partial\, \Delta G(r)}{\partial r} = 0 \quad ; \quad \frac{\partial}{\partial r}\left[\frac{1}{4\pi\varepsilon_0\varepsilon_r}\frac{-q^2}{r} + U(r) - k_B T \ln(4\pi r^2)\right] = 0. \tag{3}$$

where q is the charge on the ions and takes the value 2 in the present case. If we assume that that the non-electrostatic interaction (which is likely to be predominately due to van der Waals attraction), *U(r)*, can be neglected at such a distance, it can be easily shown that in the case of divalent cations immersed in a medium with relative dielectric constant ε_r=79.6 (again equivalent to SPC/Fw at 298.15K) the radius for the maximum is given by:

$$R_{max} = \frac{1}{4\pi\varepsilon_0\varepsilon_r}\frac{q^2}{2k_BT} \approx 14 \text{ Å}. \quad (4)$$

R_{max} could therefore be regarded as the threshold distance beyond which the ion-pair can be safely considered dissociated. Alternatively one could use the Bjerrum length as the distance beyond which the ions can be considered unbound. The Bjerrum length takes its name of the scientist who pioneered the theory of dilute electrolytes in the early 1900s[69] and it is defined as the distance at which the electrostatic interaction equals the thermal energy (k_BT), which for divalent ions is ~28 Å. In order to reduce the computational cost of the free energy calculations we limited our metadynamics pairing free energy calculations to a maximum X-$CO_3^=$ distance of 20 Å, therefore in Table 4 we report the dissociation barriers as the free energy differences between the most stable CIP configurations and R_{max}. However, by examining the analytic and computational solution of the pairing free energy problem for two ideal point particles (Fig. SI2) it is evident that the free energy between 14 Å and 28 Å changes by less than 1 kJ/mol, which is well within the accuracy of our calculations.

In a further alternative, one could use a more rigorous approach by following in the steps of Bjerrum and Fuoss[69] who showed that the dissociation constant of an ion-pair can be obtained by direct integration of the potential of mean force $\phi(r)$. Bjerrum and Fuoss assumed that a dilute electrolyte solution could be simply described as finite size particles immersed in a continuum dielectric medium, which led them to the expression for the dissociation constant;

$$K_{dis} = 4\pi C_0 \int_{R_0}^{R_1} \exp\left(-\phi(r)/k_BT\right) r^2\, dr. \quad (6)$$

where R_1 is the distance at which the ion-pairs can be regarded as dissociated, R_0 is the minimum distance at which the ions can be found and C_0 is a constant necessary to convert the concentration from the simulation units ($Å^{-3}$) to the standard units (mol/dm^3). A similar approach was used by Chialvo *et al*.[70] In ref 69 the potential of mean force was obtained analytically by assuming only a screened electrostatic interaction between the ions and the minimum cation-anion distance was regarded as a fitting parameter. However, from our metadynamics calculations we have access to the all-atom pairing free energy profiles and we therefore calculate the dissociation constant by using them instead of the analytic potential of mean force obtained from a continuum approximation. In order to derive the potential of mean force, $\Delta\phi(r)$, from the 2D free energy profiles we performed a dimensional reduction by taking a thermodynamic average along the coordination number and then used the relationship between the potential of mean force and the free energy:

$$\Delta G(r) = \phi(r) - k_B T \ln(4\pi r^2). \tag{7}$$

For the lower limit in the integral in Eq. (6) we choose R_0= 2 Å, although the calculated dissociation constants are not very sensitive to the actual value, provided it is sufficiently small. It is worth nothing here that the free energy profiles obtained from MD simulations are usually defined to within an additive constant, which cancels out when free energy differences are calculated. However, in the present case, because of the presence of a definite integral in Eq. (6) the actual value of this energy offset is important for the calculation of the dissociation constant. Hence, in order to have the correct asymptotic limit for $\Delta\phi(r)$ we have offset all the free energy curves calculated with metadynamics to overlap with the analytic limit of the free energy for

distances between 10 and 14 Å (Figure 3). We also tested that the results depend little on the upper bound of the integral, with the calculated pK_{dis} changing by less than 0.01 if R_1 is reduced from 28 Å (Bjerrum length) to 11 Å.

In the case of Mg^{2+}, given the large hidden free energy barrier separating the CIP and the SSHIP, one could argue that a lot of information is lost by using the 1D free energy profile in Eq.6, which could lead to a discrepancy in the results. However, the separation between the CIP, SSHIP and SSIP in the collective variable space is so sharp that it allows us to study the SSHIP-dissociated ions and the CIP-SSHIP equilibria separately with confidence that we are not introducing artifacts by imposing boundaries between the various states. The first equilibrium can be simply obtained by using Eq.6 with a 1D free energy profile calculated by excluding all the Gaussians corresponding to a coordination number smaller than 6 and we obtained $pK_{dis}^{SSHIP} = 2.0$. Analogously, by excluding all the Gaussians corresponding to Mg-C distances larger than 6 Å we can obtain a 1D free energy profile for the CIP-SSHIP equilibrium along the coordination number. We can then use the ratio between the probabilities of the system to be in either of the two states;

$$K_{dis}^{CIP-SSHIP} = \frac{\int_6^7 \exp\left(-\Delta G(c)/k_B T\right) \mathrm{d}c}{\int_5^6 \exp\left(-\Delta G(c)/k_B T\right) \mathrm{d}c} = \tag{7}$$

to calculate equilibrium constant for that process, which gives $pK_{dis}^{CIP-SSHIP} = 2.3$. In Eq. 7 the integral is now performed along the coordination number CV (c), with the integration limits set so as to bound the CIP and SSHIP minima. Combining these two equilibrium constants we get an overall pK_{dis} of 4.3, reported in parenthesis in Table 4.

Comparing the experimental estimates of the pairing free energy with the predictions from our simulations, we note that agreement is good for Ca^{2+}, Sr^{2+} and Ba^{2+} (differences < 5 kJ/mol) while for Mg^{2+} there is a substantial discrepancy (>10 kJ/mol). This is somewhat surprising since the force field parameters for all the species have been fitted by including the solubility of the minerals, which critically depends on the ion-ion and ion-water interactions. Although it is impossible to completely discount that this could be a flaw of the force field, despite careful consideration of the thermodynamics during its derivation, we believe this is unlikely to be the complete explanation. This conjecture is supported by the observation that in order to change the force field parameters to get an accurate equilibrium constant using the Bjerrum and Fuoss approach we would have to hugely destabilize the CIP, which can be achieved by either increasing the Mg^{2+} carbonate repulsion and/or reducing the Mg^{2+} hydration free energy. However, such changes would either cause a dramatic degradation of the properties of the solid mineral phases or completely change the hydration free energy of the isolated Mg^{2+} ion. Indeed, the extent of the change would have to be so large as to make Mg^{2+} almost the same as Ca^{2+} within the force field model; something that seems unlikely to be realistic.

Instead we argue that there may instead be genuine physical reasons for the above disagreement in the ion-pairing free energy for Mg^{2+}. In this case a key factor could be the slow water dynamics around the cation leading to the large free energy barrier separating the CIP and the SSHIP, which makes both states long-lived, while in comparison the remaining dissociation is a fast process. Therefore, the experimental techniques employed to measure the dissociation constant by indirectly probing the free ion concentrations might be sensitive to this equilibrium, instead of to the full dissociation, as defined by the ions to be separated by more than R_B. On the

other hand, further equilibria leading to pre-nucleation species, not accounted for in the experimental data analysis, could also contribute to this discrepancy. Finally, it is worth mentioning that the lack of polarization in our model might lead to an underestimation of the stability of the SSHIP, where one or more water molecules are sandwiched between Mg^{2+} and $CO_3^{=}$ and could be highly polarized. However, this is open to debate and requires accurate high level *ab initio* quantum mechanics to resolve, and will be the focus of future work.

CONCLUSIONS

In conclusion, we have developed and characterized a thermodynamically consistent set of force field parameters to describe the early stages of aggregation of alkaline-earth cations with carbonate in water. The force field was calibrated against structural (crystal structures) and thermodynamic (solubility and hydration free energy) data and accurately reproduces experimental dynamic and thermodynamic properties of the ions, many of which were not included in the training set. While the results for the thermodynamics of ion-pairing with carbonate show some discrepancy with respect to experiment, it is proposed that this could partially reflect uncertainty with regard to the molecular process whose equilibrium is being measured rather than solely an error in the parameterization of the simulation. In the case of magnesium, it is possible that the measured equilibrium involves the solvent-shared ion-pair, thereby explaining the similarity of the experimental results for Ca^{2+} and Mg^{2+}, which would be unexpected based on the thermodynamics of the contact ion-pair.

The current new force field parameterization now makes it possible to extend previous simulations of calcium carbonate ion aggregation in solution to other alkaline-earth metals. In turn this makes it feasible in future studies to address the

question of whether pre-nucleation species may also exist for alkaline-earth metals other than calcium, as well as probing systems containing mixtures of different cations, such as Ca^{2+} and Mg^{2+} that are of relevant to issues such as the stabilization of amorphous calcium carbonate by impurities and the formation of dolomite.

ASSOCIATED CONTENT

Supporting Information. Full set of force field parameters in LAMMPS format, comparison between experimental and calculated water pair distribution function, free energy barrier for the water exchange at Mg2+, hydration free energy as a function of temperature, pair distribution function for the all-atom simulations compared with a model system and analytic solution of the same problem, cation-water radial distribution function, dielectric constant of SPC/fw water as a function of temperature and carbonate water pair distribution function. This material is available free of charge via the Internet at https:/pubs.acs.org.

AUTHOR INFORMATION

Corresponding Authors

*p.raiteri@curtin.edu.au

Author Contributions

The manuscript was written with contributions from all authors. All authors have given approval to the final version of the manuscript.

Funding Sources

Australian Research Council (DP0986999 and FT130100463).

ACKNOWLEDGMENT

PR and JDG would like to thank the ARC for funding (DP0986999 and FT130100463) and RD thanks Curtin University for an Early Career Research Fellowship. This work was supported by resources provided by the Pawsey Supercomputing Centre with funding from the Australian Government and the Government of Western Australia and with the assistance of resources from the National Computational Infrastructure (NCI), which is also supported by the Australian Government.

Table 1. Force field parameters for the interactions between the alkaline-earth cations and oxygen of water (O_w) and that of carbonate (O_c). The parameters for Mg^{2+}, Sr^{2+} and Ba^{2+} are those developed in the present work, while those for Ca^{2+} are taken from our previous work[3] and are given for comparison. A cut-off of 9 Å is used for all short-range potentials with a taper function applied over the last 3 Å. Parameters for water are those of the SPC/Fw model,[28] while for carbonate details can also found in our previous works,[3] except for the O_c-H_w repulsive potential that has been modified in the current study. A full tabulation of the force field parameters in LAMMPS format can be found in the Supplementary Information.

Buckingham		A (eV)	ρ (Å)	C (eV Å^6)
Mg	O_c	3944.8613	0.238160	0.0
Ca	O_c	3161.6335	0.271511	0.0
Sr	O_c	14250.269	0.244116	0.0
Ba	O_c	13478.151	0.258299	0.0
O_c	O_c	63840.199	0.198913	27.89901
O_c	O_w	12534.455133	0.202	0.0
O_c	H_w	340.0	0.217	0.0
Lennard-Jones		ϵ (eV)	σ (Å)	
Mg	O_w	0.001137	2.82	
Ca	O_w	0.000950	3.35	
Sr	O_w	0.000776	3.65	
Ba	O_w	0.000657	3.965	

Table 2. Comparison of the experimental and calculated structure and properties of the alkaline-earth metal carbonate phases. The lattice parameters at 300 K correspond to average values obtained from a 4 ns NPT run at 1 atm using a 3,360 atom simulation cell. The linear thermal expansion coefficients have been calculated by running 5 ns long NPT simulations at 5 temperatures between 100 K and 500 K while the cell angles were kept fixed.

	Experiment	Calculated 0 K	Calculated 300 K
Magnesite			
a (Å)	4.6339	4.6114	4.615
c (Å)	15.0177	15.0687	15.165
α_a (10^{-6} K^{-1})	6.75[35]		3.7
α_c (10^{-6} K^{-1})	22.9[35]		23.1
K (GPa)	108	143	
ΔG_{dis} (kJ/mol)	+44.8[68] / +44.5[71]	+44.6	
Dolomite			
a (Å)	4.8064	4.7912	4.794
c (Å)	16.006	15.9244	16.026
α_a (10^{-6} K^{-1})	6.2[36]		3.1
α_c (10^{-6} K^{-1})	25.8[36]		24.4
K (GPa)	94	107	
ΔG_{dis} (kJ/mol)	+48.7[49]	+47.3	
Calcite			
a (Å)	4.991	4.9398	4.935
c (Å)	17.062	17.1013	17.221
α_a (10^{-6} K^{-1})	-2.8[35]		-2.1
α_c (10^{-6} K^{-1})	32.3[35]		26.2
K (GPa)	67	85	
ΔG_{dis} (kJ/mol)	+48.1/+48.5[68]	+ 45.1	
Aragonite			
a (Å)	4.961	4.988	4.995
b (Å)	7.967	7.992	8.024
c (Å)	5.741	5.534	5.601
α_a (10^{-6} K^{-1})	9.1[35]		4.8
α_b (10^{-6} K^{-1})	18.8[35]		14.7
α_c (10^{-6} K^{-1})	37.1[35]		42.7
K (GPa)	65[72]	75	
ΔG_{dis} (kJ/mol)	+47.7/+47.3[68]	+44.1	
Strontianite			
a (Å)	5.1075	5.1319	5.142
b (Å)	8.4138	8.4368	8.450
c (Å)	6.0269	6.0008	6.066
α_a (10^{-6} K^{-1})	12.7[73]		6.7
α_b (10^{-6} K^{-1})	12.8[73]		6.2
α_c (10^{-6} K^{-1})	43.1[73]		40.6

K (GPa)	58	64	
ΔG_{dis} (kJ/mol)	+52.9[74]	+51.3	
Witherite			
a (Å)	5.316	5.2970	5.308
b (Å)	8.892	8.7789	8.799
c (Å)	6.428	6.5059	6.568
α_a (10^{-6} °C)	10.5[73]		6.7
α_b (10^{-6} °C)	6.0[73]		8.0
α_c (10^{-6} °C)	48.0[73]		36.4
K (GPa)	50.4	57.3	
ΔG_{dis} (kJ/mol)	+48.9[75]	+50.1	

Table 3. Comparison of the experimental and calculated properties of the alkaline-earth cations and carbonate in aqueous solution. Here $r_{X\text{-}Ow}$ is the metal-oxygen distance in the first hydration shell, CN is the coordination number of the species by water, τ represents the time scale for water exchange in the first solvent shell, and D_0 is the diffusion coefficient of the ion in water. [a]From our simulations the first peak of the carbon hydrogen pair distribution function is a convolution of two very close peaks (see Supplementary Information).

	Exp.	Previous simulations	This work
Mg^{2+}			
ΔG_{hyd}(kJ/mol)	-1768[27]	-1908[10]	-1766
ΔH_{hyd}(kJ/mol)	-1945[62]		-1876
ΔS_{hyd}(J/mol/K)	-350[62]		-368
$r_{X\text{-}Ow}$ (Å)	2.00-2.15[76]	2.2[50] / 1.98[51] / 2.31[20]	2.00
CN	6[76]	6.2[50] / 6.0[51] / 7.1[20]	6
τ (ns)	1500[59]	0.422[50] / >10 / 0.1[20]	>100
D_0 (10^{-5} cm^2/s)	0.71[77]	0.62[50]	0.86
Ca^{2+}			
ΔG_{hyd}(kJ/mol)	-1444[27]	-1593[10]	-1444
ΔH_{hyd}(kJ/mol)	-1600[62]		-1532
ΔS_{hyd}(J/mol/K)	-271[62]		-295
$r_{X\text{-}Ow}$ (Å)	2.33-2.44[76]	2.5[50] / 2.38[51]	2.36
CN	6-10[76]	8.0[50] / 6.2[19] / 7.5[20]	7.2
τ (ns)	1.1-1.6[78]	>1[50] / 0.122 / 0.049[20]	0.23
D_0 (10^{-5} cm^2/s)	0.79[77]	0.55[50] / 0.58[19]	0.95
Sr^{2+}			
ΔG_{hyd}(kJ/mol)	-1317[27]	-1448[10]	-1316
ΔH_{hyd}(kJ/mol)	-1470[62]		-1392
ΔS_{hyd}(J/mol/K)	-261[62]		-254
$r_{X\text{-}Ow}$ (Å)	2.60-2.65[76,79,80]	2.9[50] / 2.58[51]	2.55
CN	7.9-15[76,79,80]	9.1[50] / 8.0[51]	8.0
τ (ns)	1.0[81]	0.51[50] / 0.043[51]	0.36
D_0 (10^{-5} cm^2/s)	0.79[77]	0.54[50]	0.94
Ba^{2+}			
ΔG_{hyd}(kJ/mol)	-1190[27]	-1317[10]	-1185
ΔH_{hyd}(kJ/mol)	-1330[62]		-1254
ΔS_{hyd}(J/mol/K)	-224[62]		-230
$r_{X\text{-}Ow}$ (Å)	2.75-2.90[76,79,80]	2.78[51]	2.75

CN	8.1-9.5[76,79,80]	8.8[51]	8.6
τ (ns)	0.2[82]	0.015[51]	0.13
D_0 (10^{-5} cm^2/s)	0.84[77]		0.90
$CO_3^=$			
ΔG_{hyd}(kJ/mol)	-1315	-1404[20] / -1175[20]	-1312
ΔH_{hyd}(kJ/mol)	-1395		-1390
ΔS_{hyd}(J/mol/K)	-264		-260
$r_{Cc\text{-}Hw}$ (Å)	2.65[61]	1.78[19]	2.29 / 2.74[a]
$r_{Cc\text{-}Ow}$ (Å)	3.35[61]	2.69[19]	3.24
CN	9.1[61]	4.3[19]	12.1
τ (ns)		0.036[19]	0.017
D_0 (10^{-5} cm^2/s)	0.8[83]-0.955[84]	0.6[19]	1.0

Table 4. Dissociation constants and free energies for ion-pairs between the alkaline-earth cations and the carbonate anion. For Mg^{2+} we calculate the dissociation constant also by considering the CIP-SSHIP equilibrium separately from the SSHIP dissociation process (see text for the details) and this value is reported in parenthesis. For the calculated values both the results from integrating along the free energy surface, as well as direct estimation by taking differences (labeled "from FES"), are reported.

	Mg^{2+}	Ca^{2+}	Sr^{2+}	Ba^{2+}
Experimental pK_{dis} [68]	2.84-3.00	3.00-3.20	2.76	2.70
pK_{dis}	5.3 (4.3)	3.9	2.6	2.5
pK_{dis} – from FES	4.27	3.27	1.55	1.23
Experimental ΔG (kJ/mol)[68]	-16.3/-17.2	-17.2/-18.3	-15.8	-15.5
ΔG (kJ/mol)	-30.4 (-24.7)	-22.4	-14.9	-14.4
ΔG – from FES (kJ/mol)	-24.5	-18.8	-9.0	7.1

Figure 1. Self-diffusion coefficient of water and of the aqueous metal cations as a function of the simulation box size.

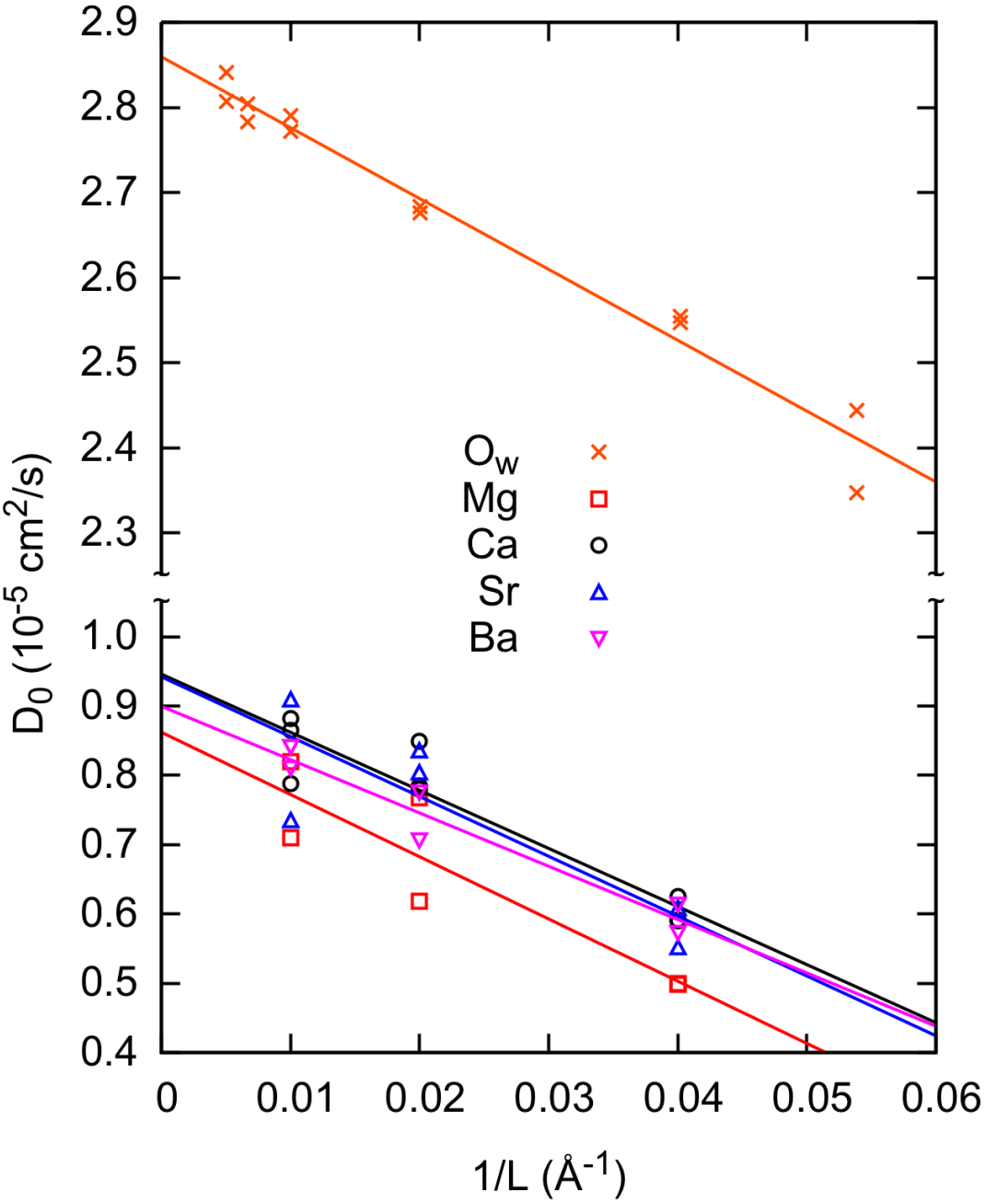

Figure 2. Free energy as a function of the water oxygen coordination number for the metal cations. The minima deviate slightly from the expected integer coordination values due to numerical factors arising from the need to define a smooth and continuous analytic definition of the coordination number for use as a collective variable (see Eq (1)).

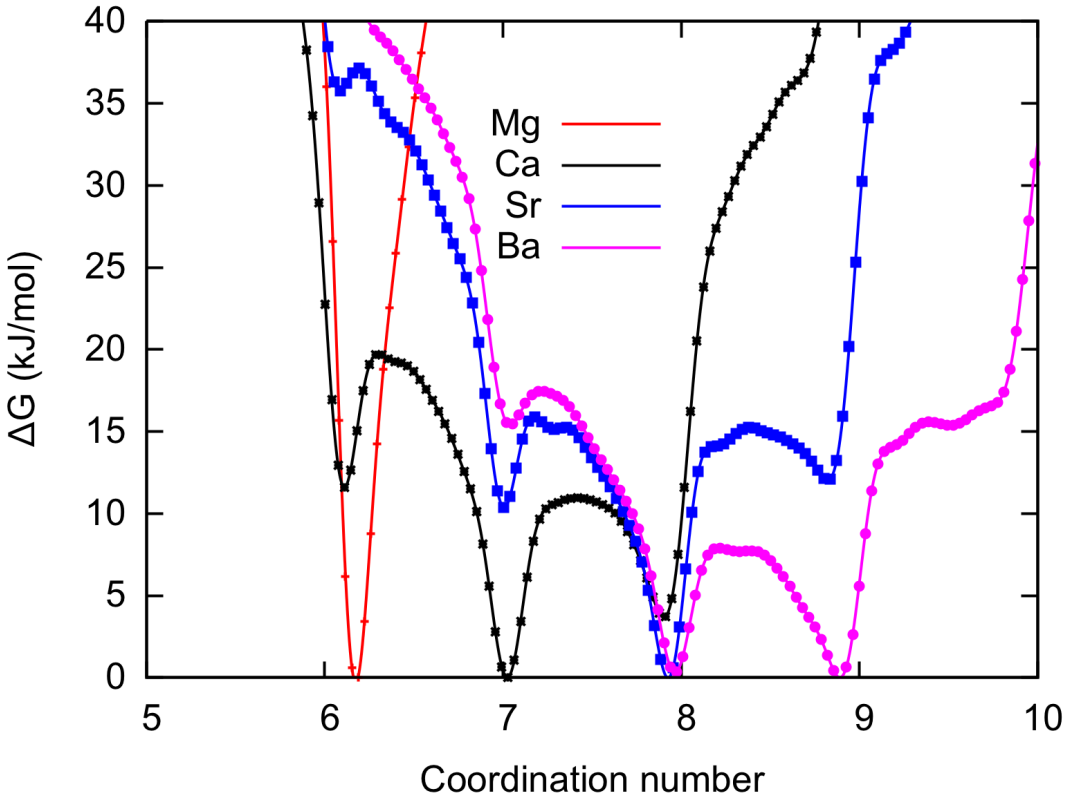

Figure 3. Metal-carbonate pairing free energy as a function of the metal-carbon distance and of the metal-water coordination number. On the Mg^{2+} plot (top left) we have overlaid letters corresponding to the panels of Figure 4, which shows representative configurations for the four free energy minima. The beads on the 2D free energy plots show the minimum free energy path for formation/dissociation of the ion-pairs. The free energy landscape is color coded according to the scale bar on the right of each panel, with the zero of energy being taken as the most stable ion-paired state.

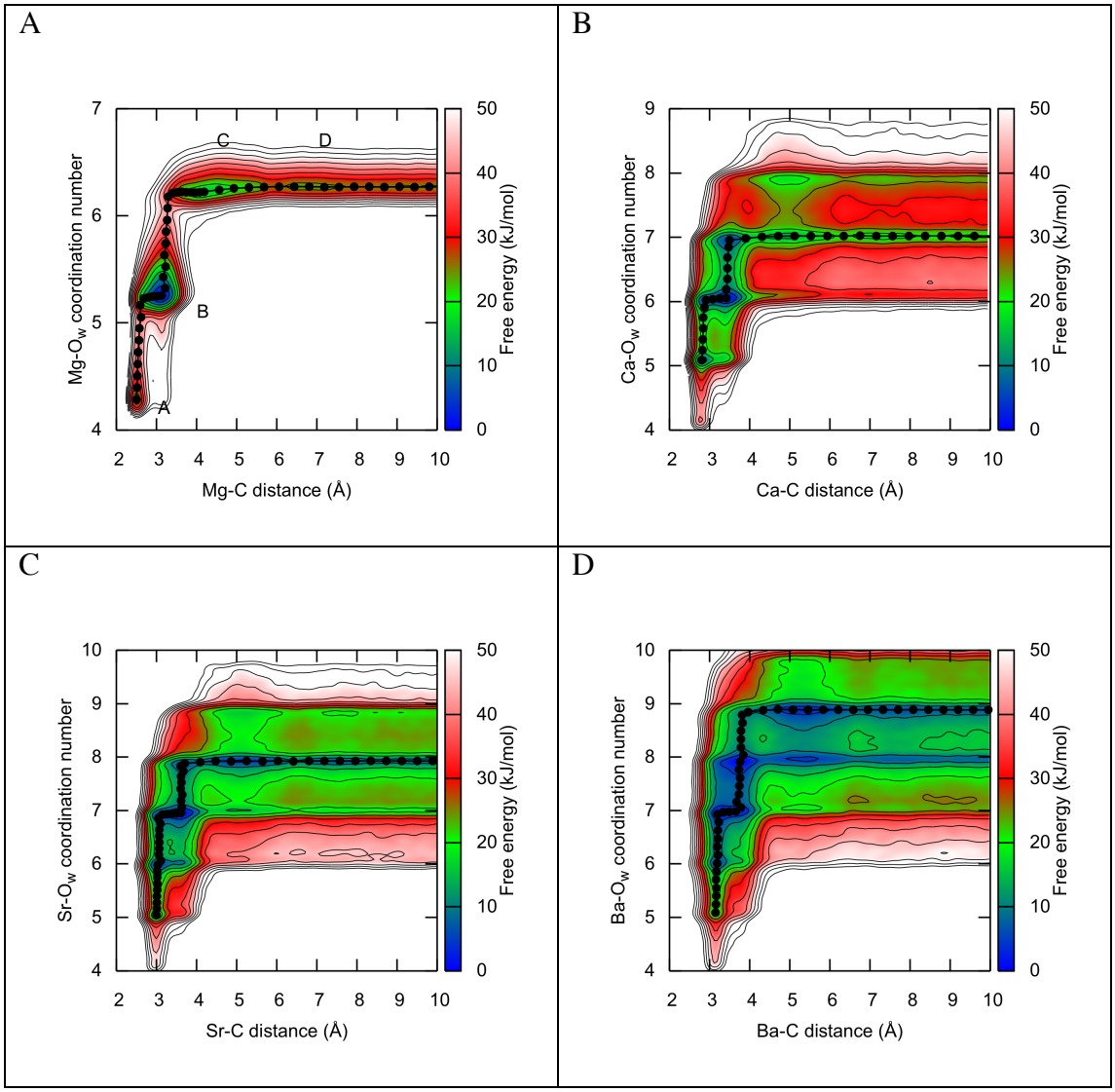

Figure 4. Representative atomic configurations of the Mg-CO_3 ion-pair: bi-dentate CIP (A), mono-dentate CIP (B), SSHIP (C) and SSIP (D); the Mg-C distances are ~2.6 Å (A), ~3.5 Å (B), ~3.9 Å(C) and ~7 Å (D). The water molecules in the carbonate hydration shell are colored in blue, while for those in the Mg hydration shell a thicker licorice representation is used with oxygen in red and hydrogen in white. The atoms of the ion-pair are shown using a ball and stick representation with Mg, C and O colored brown, cyan and red, respectively. The letters identifying the panels have also been superimposed on Fig. 3A to identify the free energy minima.

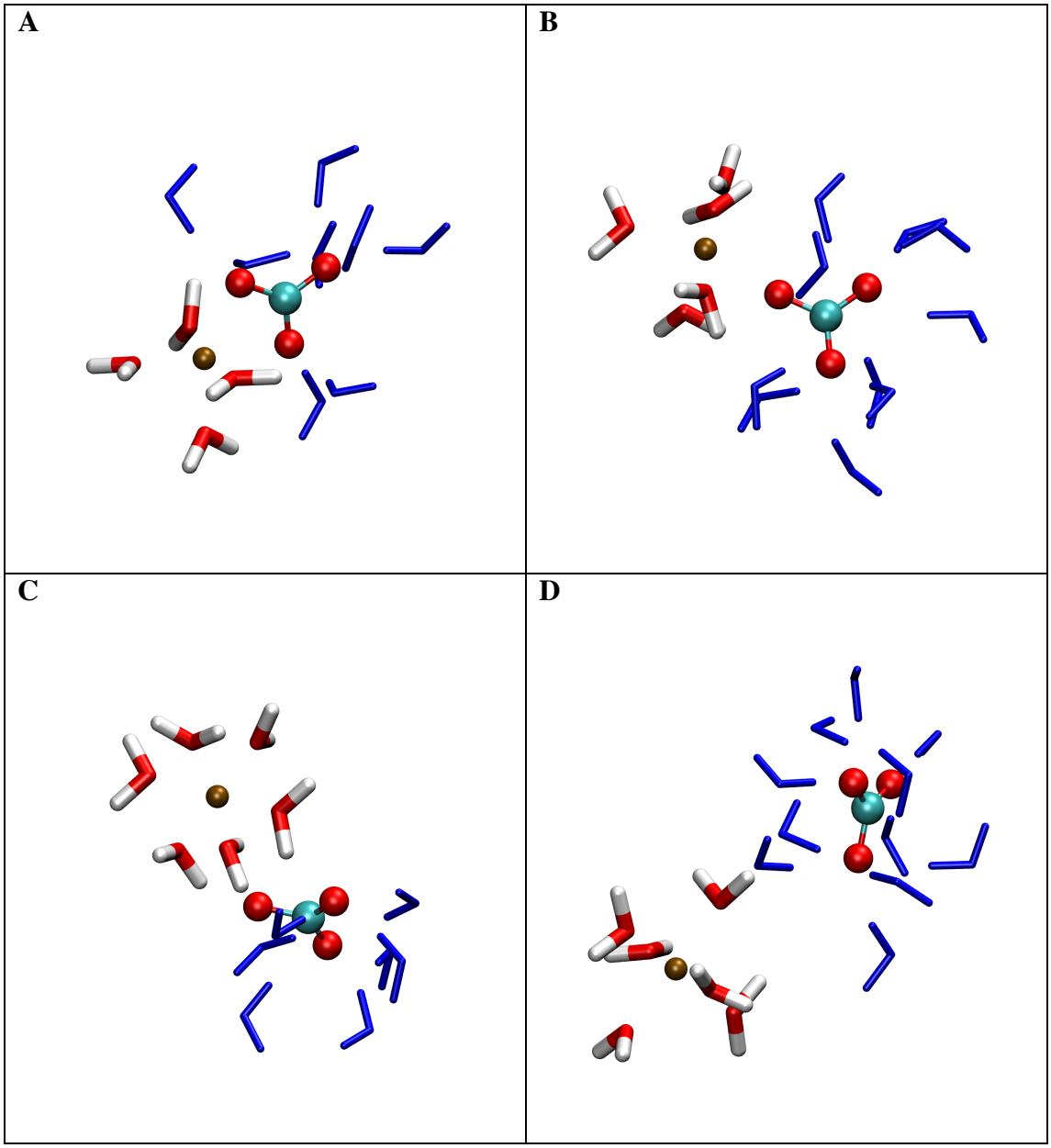

Figure 5. Projection of the 2D pairing free energy maps on to the metal-carbon distance (colored lines) with the minimum free energy path superimposed (beads) and the 1D free energy profile that would be obtained by neglecting the coordination number CV. Each colored line represents a cut through the 2D map at a specific value of the coordination number. For clarity, the 1D free energy profiles have been offset by either 10 kJ/mol (Mg^{2+} and Ca^{2+}) or 5 kJ/mol (Sr^{2+} and Ba^{2+}). The color corresponds to the free energy of the point as per the side bar, which has been kept constant in all the images.

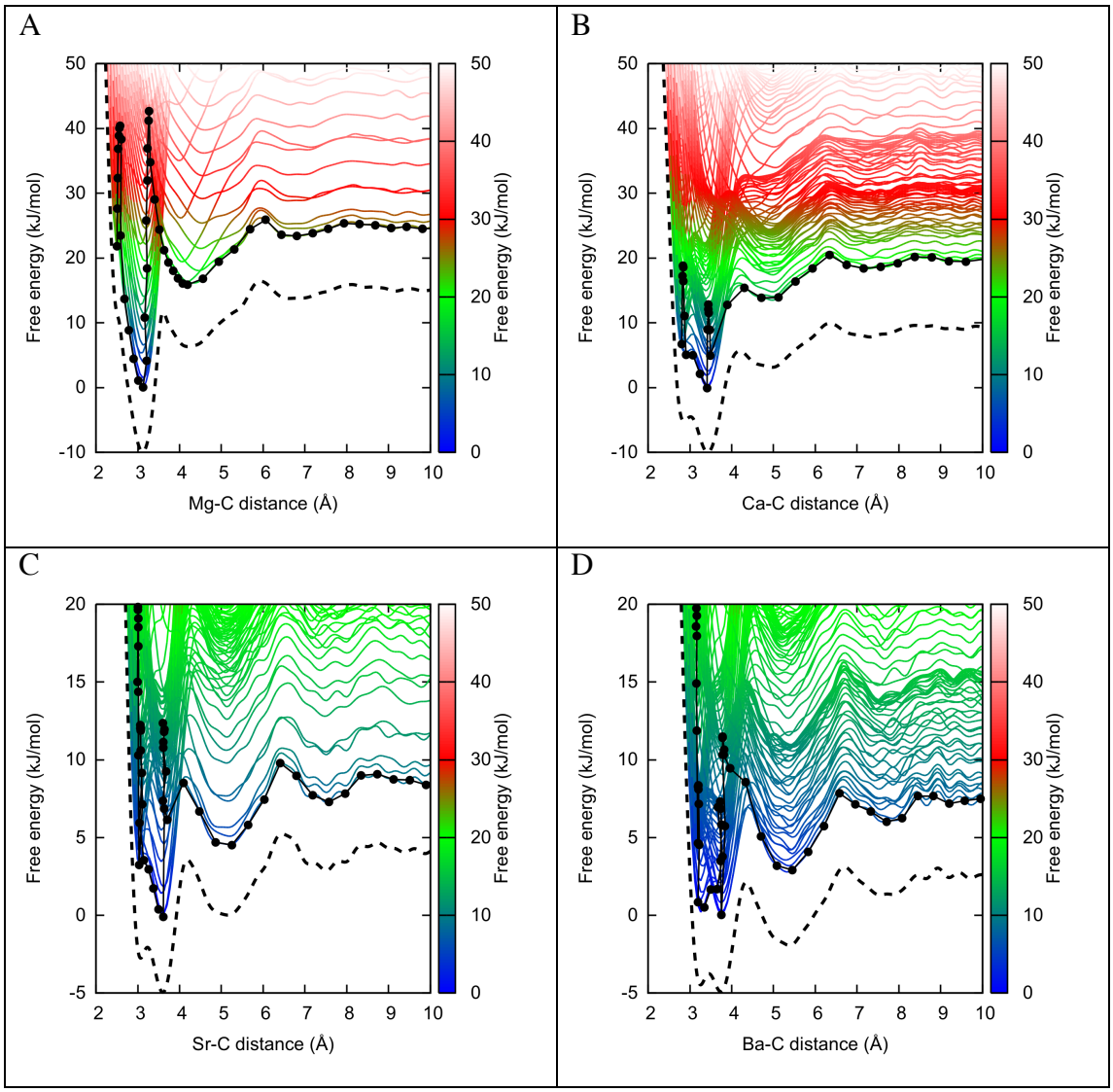

Graphical TOC

Atomic density around the $Mg^{2+}CO_3^{2-}{}_{(aq)}$ contact ion-pair in water. Red and white are used for the water oxygen and hydrogen, while cyan and pink are used for the carbon and oxygen of the carbonate ion.

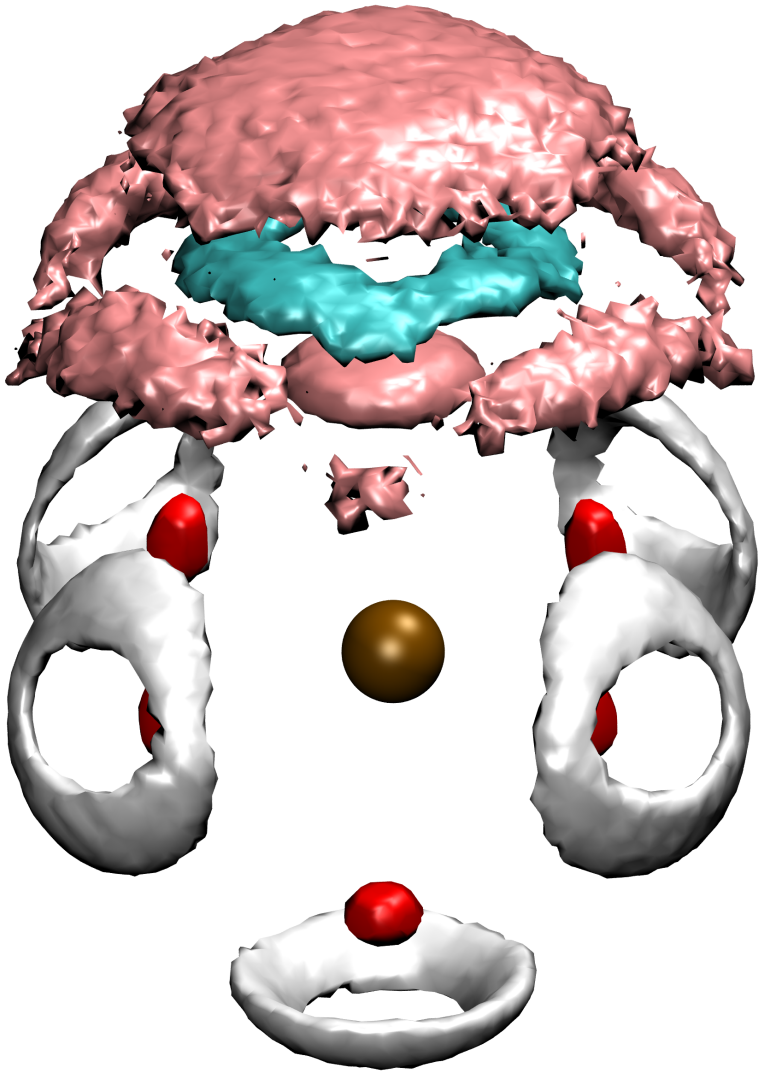

References

(1) Gebauer, D.; Voelkel, A.; Coelfen, H. Stable Prenucleation Calcium Carbonate Clusters. *Science* **2008**, *322*, 1819–1822.

(2) Gebauer, D.; Kellermeier, M.; Gale, J. D.; Bergström, L.; Cölfen, H. Pre-Nucleation Clusters as Solute Precursors in Crystallisation. *Chem. Soc. Rev.* **2014**, *43*, 2348.

(3) Demichelis, R.; Raiteri, P.; Gale, J. D.; Quigley, D.; Gebauer, D. Stable Prenucleation Mineral Clusters Are Liquid-Like Ionic Polymers. *Nat. Commun.* **2011**, *2*, 590.

(4) Yu, H.; Whitfield, T.; Harder, E.; Lamoureux, G.; Vorobyov, I.; Anisimov, V.; MacKerell, A.; Roux, B. Simulating Monovalent and Divalent Ions in Aqueous Solution Using a Drude Polarizable Force Field. *J. Chem. Theory Comput.* **2010**, *6*, 774–786.

(5) Saxena, A.; Sept, D. Multisite Ion Models That Improve Coordination and Free Energy Calculations in Molecular Dynamics Simulations. *J. Chem. Theory Comput.* **2013**, *9*, 3538–3542.

(6) Callahan, K. M.; Casillas-Ituarte, N. N.; Roeselová, M.; Allen, H. C.; Tobias, D. J. Solvation of Magnesium Dication: Molecular Dynamics Simulation and Vibrational Spectroscopic Study of Magnesium Chloride in Aqueous Solutions. *J. Phys. Chem. A* **2013**, *114*, 5141–5148.

(7) Jiao, D.; King, C.; Grossfield, A.; Darden, T. A.; Ren, P. Simulation of Ca^{2+} And Mg^{2+} Solvation Using Polarizable Atomic Multipole Potential. *J. Phys. Chem. B* **2006**, *110*, 18553–18559.

(8) Babu, C. S.; Lim, C. Empirical Force Fields for Biologically Active Divalent Metal Cations in Water. *J. Phys. Chem. A* **2006**, *110*, 691–699.

(9) Matthews, R. P.; Naidoo, K. J. Experimentally Consistent Ion Association Predicted for Metal Solutions From Free Energy Simulations. *J. Phys. Chem. B* **2010**, *114*, 7286–7293.

(10) Aqvist, J. Ion-Water Interaction Potentials Derived From Free Energy Perturbation Simulations. *J. Phys. Chem.* **1990**, *94*, 8021–8024.

(11) Pavese, A.; Catti, M.; Price, G. D.; Jackson, R. A. Interatomic Potentials for $CaCO_3$ Polymorphs (Calcite and Aragonite), Fitted to Elastic and Vibrational Data. *Phys. Chem Miner.* **1992**, *19*, 80–87.

(12) Fisler, D. K.; Gale, J. D.; Cygan, R. T. A Shell Model for the Simulation of Rhombohedral Carbonate Minerals and Their Point Defects. *Am. Mineral.* **2000**, *85*, 217–224.

(13) Hwang, S.; Blanco, M.; Goddard, W. A., III. Atomistic Simulations of Corrosion Inhibitors Adsorbed on Calcite Surfaces I. Force Field Parameters for Calcite. *J. Phys. Chem. B* **2001**, *105*, 10746–10752.

(14) Cygan, R. T.; Wright, K.; Fisler, D. K.; Gale, J. D.; Slater, B. Atomistic Models of Carbonate Minerals: Bulk and Surface Structures, Defects, and Diffusion. *Mol. Sim.* **2002**, *28*, 475–495.

(15) Archer, T.; Birse, S.; Dove, M. T.; Redfern, S.; Gale, J. D.; Cygan, R. T. An Interatomic Potential Model for Carbonates Allowing for Polarization Effects. *Phys. Chem Miner.* **2003**, *30*, 416–424.

(16) Rohl, A.; Wright, K.; Gale, J. D. Evidence From Surface Phonons for the (2× 1) Reconstruction of the (10-14) Surface of Calcite From Computer Simulation. *Am. Mineral.* **2003**, *88*, 921–925.

(17) Xiao, S.; Edwards, S. A.; Grater, F. A New Transferable Forcefield for Simulating the Mechanics of $CaCO_3$ Crystals. *J. Phys. Chem. C* **2011**, *115*,

20067–20075.
(18) de Leeuw, N. H.; Parker, S. C. Surface Structure and Morphology of Calcium Carbonate Polymorphs Calcite, Aragonite, and Vaterite: an Atomistic Approach. *J. Phys. Chem. B* **1998**, *102*, 2914–2922.
(19) Bruneval, F.; Donadio, D.; Parrinello, M. Molecular Dynamics Study of the Solvation of Calcium Carbonate in Water. *J. Phys. Chem. B* **2007**, *111*, 12219–12227.
(20) Raiteri, P.; Gale, J. D.; Quigley, D.; Rodger, P. M. Derivation of an Accurate Force-Field for Simulating the Growth of Calcium Carbonate From Aqueous Solution: a New Model for the Calcite– Water Interface. *J. Phys. Chem. C* **2010**, *114*, 5997–6010.
(21) Raiteri, P.; Gale, J. D. Water Is the Key to Nonclassical Nucleation of Amorphous Calcium Carbonate. *J. Am. Chem. Soc.* **2010**, *132*, 17623–17634.
(22) Tomono, H.; Nada, H.; Zhu, F.; Sakamoto, T.; Nishimura, T.; Kato, T. Effects of Magnesium Ions and Water Molecules on the Structure of Amorphous Calcium Carbonate: a Molecular Dynamics Study. *J. Phys. Chem. B* **2013**, *117*, 14849–14856.
(23) de Leeuw, N. H.; Parker, S. C. Molecular-Dynamics Simulation of MgO Surfaces in Liquid Water Using a Shell-Model Potential for Water. *Phys. Rev. B* **1998**, *58*, 13901–13908.
(24) Van Maaren, P. J.; Van Der Spoel, D. Molecular Dynamics Simulations of Water with Novel Shell-Model Potentials. *J. Phys. Chem. B* **2001**.
(25) Raiteri, P.; Demichelis, R.; Gale, J. D. Development of Accurate Force Fields for the Simulation of Biomineralization. *Method. Enzymol.* **2013**, *532*, 3–23.
(26) Kerisit, S.; Parker, S. C. Free Energy of Adsorption of Water and Metal Ions on the {1014} Calcite Surface. *J. Am. Chem. Soc.* **2004**, *126*, 10152–10161.
(27) David, F.; Vokhmin, V.; Ionova, G. Water Characteristics Depend on the Ionic Environment. Thermodynamics and Modelisation of the Aquo Ions. *J. Mol. Liq.* **2001**, *90*, 45–62.
(28) Wu, Y.; Tepper, H.; Voth, G. A. Flexible Simple Point-Charge Water Model with Improved Liquid-State Properties. *J. Chem. Phys.* **2006**, *124*, 024503.
(29) Plimpton, S. Fast Parallel Algorithms for Short-Range Molecular Dynamics. *J. Comput. Phys.* **1995**, *117*, 1–19.
(30) Kirkwood, J. G. Statistical Mechanics of Fluid Mixtures. *J. Chem. Phys.* **1935**, *3*, 300.
(31) Zwanzig, R. High-Temperature Equation of State by a Perturbation Method. I. Nonpolar Gases. *J. Chem. Phys.* **1954**, *22*, 1420.
(32) Hummer, G.; Pratt, L. R.; Garcia, A. Ion Sizes and Finite-Size Corrections for Ionic-Solvation Free Energies. *J. Chem. Phys.* **1997**, *107*, 9275–9277.
(33) Gale, J. D. Empirical Potential Derivation for Ionic Materials. *Phil. Mag. Part B* **1996**, *73*, 3–19.
(34) Gale, J. D.; Rohl, A. L. The General Utility Lattice Program (GULP). *Mol. Sim.* **2003**, *29*, 291–341.
(35) Markgraf, S. A.; Reeder, R. J. High-Temperature Structure Refinements of Calcite and Magnesite. *Am. Mineral.* **1985**, *70*, 590–600.
(36) Reeder, R. J.; Markgraf, S. A. High-Temperature Crystal Chemistry of Dolomite. *Am. Mineral.* **1986**, *71*, 795–804.
(37) Antao, S. M.; Hassan, I. The Orthorhombic Structure of $CaCO_3$, $SrCO_3$, $PbCO_3$ And $BaCO_3$: Linear Structural Trends. *Can. Mineral.* **2009**, *47*, 1245–1255.

(38) Holl, C. M.; Smyth, J. R.; Laustsen, H.; Jacobsen, S. D.; Downs, R. T. Compression of Witherite to 8 GPa and the Crystal Structure of BaCO3II. *Phys. Chem Miner.* **2000**, *27*, 467–473.
(39) Wang, M.; Liu, Q.; Nie, S.; Li, B.; Wu, Y.; Gao, J.; Wei, X.; Wu, X. High-Pressure Phase Transitions and Compressibilities of Aragonite-Structure Carbonates: $SrCO_3$ And $BaCO_3$. *Phys. Chem Miner.* **2015**.
(40) Fiquet, G.; Reynard, B. High-Pressure Equation of State of Magnesite: New Data and a Reappraisal. *Am. Mineral.* **1999**.
(41) Ross, N. L.; Reeder, R. J. High-Pressure Structural Study of Dolomite and Ankerite. *Am. Mineral.* **1992**, *77*, 412–421.
(42) Zhang, J.; Reeder, R. J. Comparative Compressibilities of Calcite-Structure Carbonates: Deviations From Empirical Relations. *Am. Mineral.* **1999**, *84*, 861–870.
(43) Shinoda, W.; Shiga, M.; Mikami, M. Rapid Estimation of Elastic Constants by Molecular Dynamics Simulation Under Constant Stress. *Phys. Rev. B* **2004**, *69*, 134103.
(44) Tuckerman, M. E.; Alejandre, J.; López-Rendón, R.; Jochim, A. L.; Martyna, G. J. A Liouville-Operator Derived Measure-Preserving Integrator for Molecular Dynamics Simulations in the Isothermal–Isobaric Ensemble. *J. Phys. A-Math. Gen.* **2006**, *39*, 5629.
(45) Tribello, G. A.; Bonomi, M.; Branduardi, D.; Camilloni, C.; Bussi, G. Computer Physics Communications. *Comput. Phys. Commun.* **2014**, *185*, 604–613.
(46) Laio, A.; Parrinello, M. Escaping Free-Energy Minima. *P. Natl. Acad. Sci. USA* **2002**, *99*, 12562–12566.
(47) Raiteri, P.; Laio, A.; Gervasio, F. L.; Micheletti, C.; Parrinello, M. Efficient Reconstruction of Complex Free Energy Landscapes by Multiple Walkers Metadynamics. *J. Phys. Chem. B* **2006**, *110*, 3533–3539.
(48) Barducci, A.; Bussi, G.; Parrinello, M. Well-Tempered Metadynamics: a Smoothly Converging and Tunable Free-Energy Method. *Phys. Rev. Lett.* **2008**, *100*, 20603.
(49) Langmuir, D. *Aqueous Environmental Geochemistry*; Prentice-Hall: Upper Saddle River, New Jersey, 1997.
(50) Obst, S.; Bradaczek, H. Molecular Dynamics Study of the Structure and Dynamics of the Hydration Shell of Alkaline and Alkaline-Earth Metal Cations. *J. Phys. Chem.* **1996**, *100*, 15677–15687.
(51) Larentzos, J. P.; Criscenti, L. J. A Molecular Dynamics Study of Alkaline Earth Metal–Chloride Complexation in Aqueous Solution. *J. Phys. Chem. B* **2008**, *112*, 14243–14250.
(52) Yang, Z.-Z.; Li, X. Molecular-Dynamics Simulations of Alkaline-Earth Metal Cations in Water by Atom-Bond Electronegativity Equalization Method Fused Into Molecular Mechanics. *J. Chem. Phys.* **2005**, *123*, 094507.
(53) Freeman, C. L.; Harding, J. H.; Cooke, D. J.; Elliott, J. A.; Lardge, J. S.; Duffy, D. M. New Forcefields for Modeling Biomineralization Processes. *J. Phys. Chem. C* **2007**, *111*, 11943–11951.
(54) Chaudhari, M. I.; Soniat, M.; Rempe, S. B. Octa-Coordination and the Aqueous Ba^{2+} Ion. *J. Phys. Chem. B* **2015**, *119*, 8746–8753.
(55) Allen, R. J.; Frenkel, D.; Wolde, ten, P. R. Forward Flux Sampling-Type Schemes for Simulating Rare Events: Efficiency Analysis. *J. Chem. Phys.* **2006**, *124*, 194111.

(56) Allen, R. J.; Valeriani, C. Forward Flux Sampling for Rare Event Simulations. *J. Phys.: Condens. Matter* **2009**.
(57) Tiwary, P.; Parrinello, M. From Metadynamics to Dynamics. *Phys. Rev. Lett.* **2013**, *111*, 230602.
(58) Allnér, O.; Nilsson, L.; Villa, A. Magnesium Ion–Water Coordination and Exchange in Biomolecular Simulations. *J. Chem. Theory Comput.* **2012**, *8*, 1493–1502.
(59) Bleuzen, A.; Pittet, P. A.; Helm, L.; Merbach, A. E. Water Exchange on Magnesium (II) in Aqueous Solution: a Variable Temperature and Pressure ^{17}O NMR Study. *Magn. Reson. Chem.* **1997**, *35*, 765–773.
(60) Yeh, I.; Hummer, G. System-Size Dependence of Diffusion Coefficients and Viscosities From Molecular Dynamics Simulations with Periodic Boundary Conditions. *J. Phys. Chem. B* **2004**, *108*, 15873–15879.
(61) Kameda, Y.; Sasaki, M.; Hino, S.; Amo, Y.; Usuki, T. Neutron Diffraction Study on the Hydration Structure of Carbonate Ion by Means of 12C/13C Isotopic Substitution Method. *Physica B* **2006**, *385-386*, 279–281.
(62) Marcus, Y. A Simple Empirical Model Describing the Thermodynamics of Hydration of Ions of Widely Varying Charges, Sizes, and Shapes. *Biophys. Chem.* **1994**, *51*, 111–127.
(63) di Tommaso, D.; de Leeuw, N. H. First Principles Simulations of the Structural and Dynamical Properties of Hydrated Metal Ions Me 2+and Solvated Metal Carbonates (Me = Ca, Mg, and Sr). *Cryst. Growth Des.* **2010**, *10*, 4292–4302.
(64) E, W.; Ren, W.; Vanden-Eijnden, E. Finite Temperature String Method for the Study of Rare Events. *J. Phys. Chem. B* **2005**, *109*, 6688–6693.
(65) Vanden-Eijnden, E.; Venturoli, M. Revisiting the Finite Temperature String Method for the Calculation of Reaction Tubes and Free Energies. *J. Chem. Phys.* **2009**, *130*, 194103.
(66) Dellago, C.; Bolhuis, P. G.; Csajka, F. S.; Chandler, D. Transition Path Sampling and the Calculation of Rate Constants. *J. Chem. Phys.* **1998**, *108*, 1964–1977.
(67) Hefter, G. When Spectroscopy Fails: the Measurement of Ion Pairing. *Pure Appl. Chem.* **2006**, *78*, 1571–1586.
(68) De Visscher, A.; Vanderdeelen, J.; Königsberger, E.; Churagulov, B. R.; Ichikuni, M.; Tsurumi, M. IUPAC-NIST Solubility Data Series. 95. Alkaline Earth Carbonates in Aqueous Systems. Part 1. Introduction, Be and Mg. *J. Phys. Chem. Ref. Data* **2012**, *41*, 013105.
(69) Fuoss, R. M.; Kraus, C. A. Properties of Electrolytic Solutions. III. the Dissociation Constant. *J. Am. Chem. Soc.* **1933**, *55*, 1019–1028.
(70) Chialvo, A.; Cummings, P.; Cochran, H.; Simonson, J.; Mesmer, R. Na^+–Cl^- Ion Pair Association in Supercritical Water. *J. Chem. Phys.* **1995**, *103*, 9379–9387.
(71) Bénézeth, P.; Saldi, G. D.; Dandurand, J.-L.; Schott, J. Chemical Geology. *Chem. Geol.* **2011**, *286*, 21–31.
(72) Martinez, I.; Zhang, J.; Reeder, R. J. In Situ X-Ray Diffraction of Aragonite and Dolomite at High Pressure and High Temperature; Evidence for Dolomite Breakdown to Aragonite and Magnesite. *Am. Mineral.* **1996**, *81*, 611–624.
(73) Ye, Y.; Smyth, J. R.; Boni, P. Crystal Structure and Thermal Expansion of Aragonite-Group Carbonates by Single-Crystal X-Ray Diffraction. *Am.*

Mineral. **2012**, *97*, 707–712.
(74) Busenberg, E.; Plummer, L. N.; Parker, V. B. The Solubility of Strontianite ($SrCO_3$) In CO_2-H_2O Solutions Between 2 and 91°C, the Association Constants of $SrHCO^+_3$(Aq) and $SrCO^0_3$(Aq) Between 5 and 80° C, and an Evaluation of the Thermodynamic Properties of Sr^{2+}(Aq) and $SrCO_3$(Cr) Ad 1 Atm Total Pressure. *Geochim. Cosmochim. Ac*. **1984**, *48*, 2021–2035.
(75) Busenberg, E.; Plummer, N. L. The Solubility of $BaCO_3$ (Cr)(Witherite) in CO_2-H_2O Solutions Between 0 and 90 C, Evaluation of the Association Constants of $BaHCO^+_3$(Aq) and $BaCO^0_3$ (Aq) Between 5 and 80 C, and a Preliminary Evaluation of the Thermodynamic Properties of Ba^{2+}(Aq). *Geochim. Cosmochim. Ac*. **1986**, *50*, 2225–2233.
(76) Ohtaki, H.; Radnai, T. Structure and Dynamics of Hydrated Ions. *Chem. Rev*. **1993**, *93*, 1157–1204.
(77) *Self Diffusion in Electrolite Solutions: a Critical Examination of Data Compiled From the Literature*.; Mills, R.; Lobo, V. M. M., Eds.; Elsevier.
(78) Atkinson, G.; Emara, M. M.; Fernandez-Prini, R. Ultrasonic Absorption in Aqueous Solutions of Calcium Acetate and Other Bivalent Metal Acetates. *J. Phys. Chem*. **1974**, *78*, 1913–1917.
(79) Persson, I.; Sandstrom, M.; Yokoyama, H.; Chaudhry, M. Structure of the Solvated Strontium and Barium Ions in Aqueous, Dimethyl Sulfoxide and Pyridine Solution, and Crystal Structure of Strontium and Barium Hydroxide Octahydrate. *Z Naturforsch* **1995**, *50*, 21–37.
(80) D'Angelo, P.; Pavel, N.; Roccatano, D.; Nolting, H. Multielectron Excitations at the L Edges of Barium in Aqueous Solution. *Phys. Rev. B* **1996**, *54*, 12129–12138.
(81) Helm, L.; Merbach, A. E. Water Exchange on Metal Ions: Experiments and Simulations. *Coordin. Chem. Rev*. **1999**, *187*, 151–181.
(82) Stack, A. G.; Rustad, J. R. Structure and Dynamics of Water on Aqueous Barium Ion and the {001} Barite Surface. *J. Phys. Chem. C* **2007**, *111*, 16387–16391.
(83) Kigoshi, K.; Hashitani, T. The Self-Diffusion Coefficients of Carbon Dioxide, Hydrogen Carbonate Ions and Carbonate Ions in Aqueous Solutions. *B. Chem. Soc. Jpn*. **1963**, *36*, 1372.
(84) Li, Y.; Gregory, S. Diffusion of Ions in Sea Water and in Deep-Sea Sediments. *Geochim. Cosmochim. Ac*. **1974**, *38*, 703–714.